Publication VI

Ilkka Laakso, Tero Uusitupa, and Sami Ilvonen. 2010. Comparison of SAR calculation algorithms for the finite-difference time-domain method. Physics in Medicine and Biology, volume 55, number 15, pages N421-N431.

IOP PUBLISHING PHYSICS IN MEDICINE AND BIOLOGY

Phys. Med. Biol. **55** (2010) N421–N431 doi:10.1088/0031-9155/55/15/N03

NOTE

Comparison of SAR calculation algorithms for the finite-difference time-domain method

Ilkka Laakso, Tero Uusitupa and Sami Ilvonen

Department of Radio Science and Engineering, Aalto University, Otakaari 5 A, 02150 Espoo, Finland

E-mail: ilkka.laakso@tkk.fi

Received 17 March 2010, in final form 29 June 2010
Published 20 July 2010
Online at stacks.iop.org/PMB/55/N421

Abstract

Finite-difference time-domain (FDTD) simulations of specific-absorption rate (SAR) have several uncertainty factors. For example, significantly varying SAR values may result from the use of different algorithms for determining the SAR from the FDTD electric field. The objective of this paper is to rigorously study the divergence of SAR values due to different SAR calculation algorithms and to examine if some SAR calculation algorithm should be preferred over others. For this purpose, numerical FDTD results are compared to analytical solutions in a one-dimensional layered model and a three-dimensional spherical object. Additionally, the implications of SAR calculation algorithms for dosimetry of anatomically realistic whole-body models are studied. The results show that the trapezium algorithm—based on the trapezium integration rule—is always conservative compared to the analytic solution, making it a good choice for worst-case exposure assessment. In contrast, the mid-ordinate algorithm—named after the mid-ordinate integration rule—usually underestimates the analytic SAR. The linear algorithm—which is approximately a weighted average of the two—seems to be the most accurate choice overall, typically giving the best fit with the shape of the analytic SAR distribution. For anatomically realistic models, the whole-body SAR difference between different algorithms is relatively independent of the used body model, incident direction and polarization of the plane wave. The main factors affecting the difference are cell size and frequency. The choice of the SAR calculation algorithm is an important simulation parameter in high-frequency FDTD SAR calculations, and it should be explained to allow intercomparison of the results between different studies.

(Some figures in this article are in colour only in the electronic version)

1. Introduction

The finite-difference time-domain (FDTD) method is the most widely used method in the computational dosimetry of radio-frequency electromagnetic fields. There are several uncertainty factors affecting the reliability of the simulated specific-absorption rate (SAR) values. Some uncertainty factors are related to modelling, such as the accuracy of anatomical models or models of dielectric properties of tissues. Several factors are caused only by the computational method. One main source of uncertainty is the discretization error affected by the frequency and resolution of the FDTD grid (Laakso 2009, Dimbylow *et al* 2010). In some cases, significant error might be caused by reflection from absorbing boundary conditions (ABCs) (Wang *et al* 2006), although it is possible to make ABCs with negligibly small error (Findlay and Dimbylow 2006, Laakso *et al* 2007). Several additional sources of uncertainty have been discussed in Kühn *et al* (2009).

Recently there has been a discussion about the choice of the algorithm by which the SAR for each Yee cell is determined from the electric field produced by the FDTD method (Uusitupa *et al* 2008, Dimbylow *et al* 2008, 2010). Different algorithms for determining the SAR may produce significantly varying SAR values, especially at high frequencies or low resolution. This paper presents SAR calculations in several cases with three different SAR algorithms that are described in the following section. The objective is firstly to find out which algorithm is preferred by comparing the numerical FDTD results to analytical solutions. The studied cases include a one-dimensional layered model and a three-dimensional spherical object. Secondly, the implications of SAR calculation algorithms for dosimetry of anatomically realistic whole-body models are studied by re-calculating the results of our previous study (Uusitupa *et al* 2010), which considered plane-wave exposure from various directions in multiple different human body models including different postures.

2. SAR calculation algorithms

In the following theoretical discussion it is assumed that the fields have a sinusoidal time-dependence of the form $\tilde{A}(t) = \mathrm{Re}[A \exp(j\omega t)]$. Although complex field values A are used for the theoretical discussion, they are not needed in practice. Namely, using the presented SAR calculation algorithms, all the resulting expressions will eventually consist of real parts of products of complex numbers which may be presented in the form

$$\mathrm{Re}(AB^*) = \tilde{A}(t)\tilde{B}(t) + \tilde{A}\left(t + \frac{T}{4}\right)\tilde{B}\left(t + \frac{T}{4}\right), \tag{1}$$

where $T = 1/f$ is the period of the sinusoidal excitation. So the SAR can be calculated directly from two instantaneous values of time-domain fields without the need to determine complex field values.

The SAR is determined from the electromagnetic power-loss density by dividing with the specific gravity of the tissue. Assuming that the conductivity σ is constant inside each individual Yee cell, in the analytical case the total power loss in a single Yee cell is given by the integral

$$\frac{\sigma}{2}\int_{\mathrm{cell}} |E_x|^2 + |E_y|^2 + |E_z|^2 \,\mathrm{d}V, \tag{2}$$

from which the average power-loss density or SAR may be determined by division with the volume or mass of the cell, respectively.

The FDTD method produces an electric field which is located on the edges of the cells (figure 1) and which is affected by the discretization error. Therefore, there are varying ways

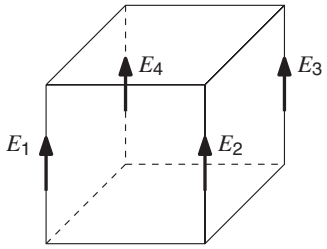

Figure 1. Electric field on the edges of the Yee cell.

to interpret the FDTD electric field, which gives rise to different ways for approximating the integral in (2), resulting in different SAR calculation algorithms. In the following, three different algorithms will be presented. They are referred to as *trapezium*, *mid-ordinate* and *linear* algorithms by their close connection with the elementary numerical integration rules. Each algorithm is based on different assumption on how to interpret the FDTD electric field.

2.1. Trapezium algorithm

The trapezium algorithm is based on the assumption that the edge-based electric field components produced by FDTD are good pointwise approximations of the accurate electric field. Because we approximately know the values of the electric field on the edges, we may now use the elementary trapezium integration rule to approximate the integral (2). For the E_z component, for instance, the integral is approximated as

$$\int_{\text{cell}} |E_z|^2 \, \mathrm{d}V \approx \frac{\text{Volume(cell)}}{4}[|E_1|^2 + |E_2|^2 + |E_3|^2 + |E_4|^2], \tag{3}$$

where the notation is the same as in figure 1. The absolute values may be calculated from the time-domain field values by equation (1). Alternatively, they could be determined by seeking the maximum values of the corresponding time-domain absolute values over a half cycle.

There is also another way to derive the trapezium algorithm. By starting directly from the FDTD update equations, one may derive a discrete version of the Poynting theorem (de Moerloose and de Zutter 1995), according to which the resistive power-loss density s is

$$s = -\frac{1}{2}\mathrm{Re}\{\hat{D} \cdot \langle E \times H^* \rangle\} = \frac{1}{2}\langle \sigma |E|^2 \rangle \cos\frac{\omega \Delta_t}{2}, \tag{4}$$

where the centre term is the discrete analogue of the divergence of the Poynting vector and Δ_t is the time step. The factor $\langle \sigma |E|^2 \rangle$ means taking average over $\sigma |E|^2$ on the edges to the centre point of the cell[1]. The cosine factor is very close to 1 in practical dosimetry calculations, so (4) describes essentially the same averaging procedure as (3). Consequently, the trapezium algorithm gives the same whole-body averaged SAR as obtained by integrating the normal component of the discrete Poynting vector over a surface enclosing the whole human body. This was also verified numerically using one-dimensional layered objects (section 3.1).

The trapezium algorithm has been considered before in Dimbylow *et al* (2008) where it was denoted 'algorithm D', and in Uusitupa *et al* (2008) where it was called '$(E^2)_{\text{ave}}$-method'. A related algorithm, 'algorithm C' (Dimbylow *et al* 2008, 2010), always gives slightly smaller values than the trapezium algorithm.

[1] de Moerloose and de Zutter (1995) derived the formula for a corner point of a Yee cell. The case for the centre point may be derived similarly.

2.2. Mid-ordinate algorithm

In the mid-ordinate algorithm, it is assumed that the arithmetic average over the edge-based electric field components is a good approximation of the accurate electric field at the centre point of the cell. The field value at the centre point of the cell may then be used to approximate the integral (2) by the mid-ordinate integration rule, resulting in an approximation

$$\int_{\text{cell}} |E_z|^2 \, \mathrm{d}V \approx \frac{\text{Volume(cell)}}{16} |E_1 + E_2 + E_3 + E_4|^2, \tag{5}$$

which can be calculated from the time-domain fields by (1), or by seeking the maximum absolute value of the average time-domain field over a half period. The mid-ordinate algorithm always produces smaller power loss than the trapezium algorithm in all cells. In previous papers, the mid-ordinate algorithm has been called the 'twelve-components approach' (Caputa *et al* 1999), 'algorithm A' (Dimbylow *et al* 2008, 2010) or the '$(E_{\text{ave}})^2$-method' (Uusitupa *et al* 2008).

2.3. Linear algorithm

In the linear algorithm, it is assumed that the edge-based field components define a bilinear interpolant that is a good global approximation of the accurate electric field. Consequently, each complex electric field component in (2) is of the bilinear form

$$E_z(\xi, \eta) = (1 - \xi)(1 - \eta)E_1 + (1 - \xi)\eta E_2 + \xi\eta E_3 + \xi(1 - \eta)E_4, \tag{6}$$

with $0 \leqslant \xi, \eta \leqslant 1$. With this assumption the integral (2) may be calculated accurately from the field values on the edges. The integration is straightforward and results in several terms of the form (1). In one dimension the linear algorithm is exactly a weighted average (ratio 1:2) of the trapezium and mid-ordinate algorithms. So the linear algorithm resembles the Simpson numerical integration rule.

The assumption of bilinear electric field is natural because the FDTD method may be interpreted as a special case of the time-domain finite-element method (Rylander *et al* 2005) with piecewise bilinear edge-based basis functions. Using these basis functions, the electric field inside the cells is of the form (6). We have used the linear algorithm in our previous studies (Laakso 2009, Uusitupa *et al* 2010).

3. Numerical results compared to analytic solutions

In this section, it is studied which SAR calculation algorithm gives the best fit with the analytical solution in several test cases.

3.1. One-dimensional layered model

The geometry of the first case is a layered half space, consisting of skin (wet), fat (infiltrated with blood) and muscle layers (Gabriel *et al* 1996), exposed to a plane wave. A one-dimensional model is able to predict reasonably well the differences of the SAR algorithms in anatomically realistic 3D models (see figure 5). For this kind of geometry there exists a simple analytic solution. For the comparison of analytical and numerical results, the analytical power loss for each Yee cell was calculated by integration (2). This allowed not only the comparison of the total whole-body SAR but also the shape of the spatial SAR distribution by calculating the relative error of power-loss density s in l_1 norm, i.e.

$$l_1 \text{ error} = \frac{\sum_{\text{cells}} |s_{\text{FDTD}} - s_{\text{analytical}}|}{\sum_{\text{cells}} |s_{\text{analytical}}|}. \tag{7}$$

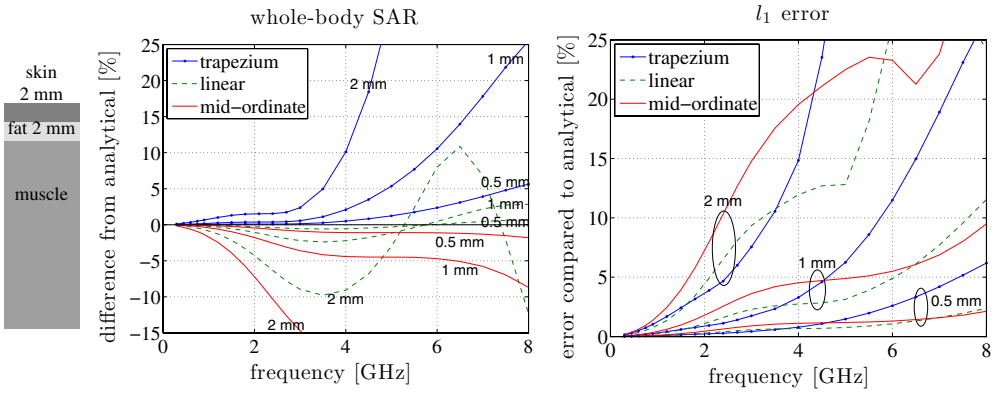

Figure 2. Numerical power loss calculated by different algorithms compared to the analytical power loss for three cell sizes (2 mm, 1 mm and 0.5 mm). The exposed geometry is depicted on the left.

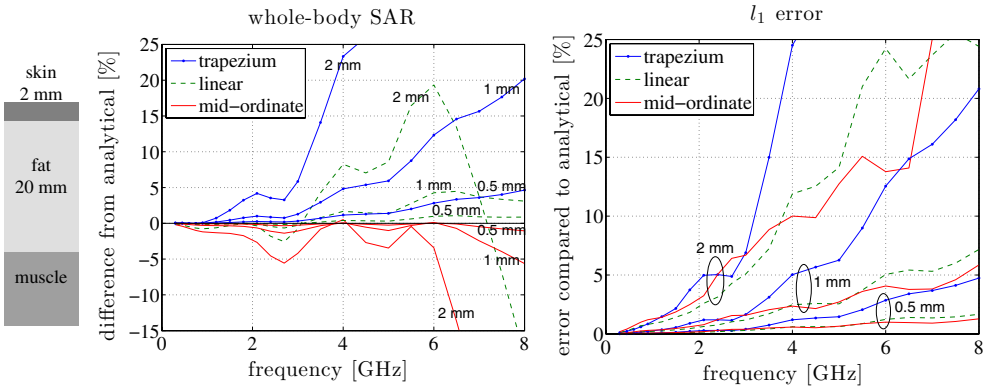

Figure 3. Numerical power loss calculated by different algorithms compared to the analytical power loss for three cell sizes (2 mm, 1 mm and 0.5 mm). The geometry is depicted on the left.

A basic one_dimensional FDTD model (Taflove and Hagness 2005) was implemented with a very thick convolutional perfectly matched layer ABC (Roden and Gedney 2000) on the left side and a very thick muscle layer on the right. The time step was chosen to be $\Delta_t = 0.99\Delta_x/c_0$. The permittivity and conductivity values on the edges of the cells were arithmetic averages over the values in the adjacent cells (this same choice was used in all 3D cases too).

Figures 2 and 3 show examples of the the numerical FDTD results compared with the analytical results for two different geometries and three resolutions. In figure 2 the thickness of both the skin and the fat layer is 2 mm. The case depicted in figure 3 is otherwise similar but the thickness of the fat layer is 20 mm. The results show that none of the three algorithms was the most accurate choice in every case. Depending on the case, each algorithm could produce the closest match with analytical SAR and the smallest l_1 error. For example, the trapezium algorithm gave the closest match with the analytical SAR in figure 2 under 3 GHz frequencies for all resolutions. However in figure 3, the mid-ordinate algorithm was the most accurate choice at 1 mm and 0.5 mm resolutions, especially at frequencies over 4 GHz.

Table 1. Average (and worst case in parenthesis) frequencies (GHz) below which l_1 error is smaller than 5%. Also included are the maximum frequencies predicted by the $\lambda/10$ rule for muscle tissue.

Algorithm/cell size	2 mm		1 mm		0.5 mm	
Trapezium	2.1	(1.9)	4.2	(3.8)	8.1	(6.9)
Linear	2.7	(2.1)	5.9	(4.7)	>10	(>10)
Mid-ordinate	2.2	(1.6)	6.3	(3.6)	>10	(7.6)
$\lambda/10$ rule for muscle	2.1		4.2		9.0	

Because of the discretization error in the FDTD method, the electric field is erroneous compared to the analytic solution. The size of the error is connected to the ratio between the cell size and the wavelength. The effects of discretization error on the performance of the SAR calculation algorithms can be seen in figures 2 and 3. By increasing the resolution, i.e. making the discretization error smaller, the whole-body SAR values calculated by each algorithm seem to converge to the analytic whole-body SAR. Also, when the cell size is halved, the l_1 error for each algorithm (and the difference between the algorithms) is reduced to approximately one-fourth. The same is true for the global error in the electric field (not shown in the figures) because power loss inside the object is directly related to the squared amplitude of the electric field.

In addition to the two example cases in figures 2 and 3, multiple cases of the same kind were simulated with fat thickness varied from 0 mm to 20 mm at 2 mm intervals. Table 1 shows the smallest frequencies at which the l_1 error exceeds 5% for each algorithm and resolution, averaged over all simulated cases. Also shown are the worst-case (minimum over all cases) frequencies, under which the l_1 error was smaller than 5% in every simulated case. As seen in table 1, the frequencies calculated by the condition that l_1 error is smaller than 5% approximately correspond to those given by the commonly used $\lambda/10$ rule of thumb. For the trapezium algorithm, the l_1 error rises the quickest at high frequencies, resulting in the lowest average applicable frequencies at 1 mm and 0.5 mm resolutions. The mid-ordinate algorithm has on average higher frequencies at 1 mm and 0.5 mm compared to the trapezium algorithm, but worst-case performance is similar to the trapezium algorithm. Overall, the linear algorithm seems to be the most robust choice; it has high average frequencies at all resolutions, and worst-case frequencies are higher compared to the other algorithms. With the linear method, a lower resolution may be used at slightly higher frequencies without losing too much accuracy.

In each of the simulated cases, the trapezium algorithm always overestimated the analytical whole-body SAR for all resolutions. The overestimation became more severe with coarser resolutions. In contrast, the mid-ordinate algorithm nearly always underestimated the whole-body averaged SAR, and the underestimation was amplified for coarser resolutions. It seems that the discretization error manifests itself in overestimation for the trapezium algorithm and in underestimation for the mid-ordinate algorithm. Hence, the mid-ordinate algorithm does not seem to be a good choice for worst-case exposure assessment. Better choices are the trapezium algorithm, which was always conservative compared to the analytic solution, or the linear algorithm, which was overall the most accurate choice.

3.2. Small spherical object

The second analytical example is a sphere that is exposed to a plane wave (figure 4). The sphere has radius 5 cm, and it is composed entirely of muscle tissue (Gabriel *et al* 1996). The

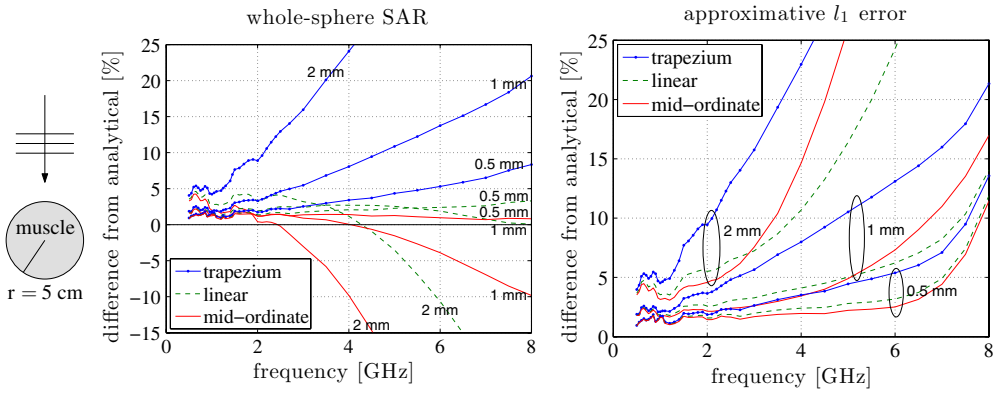

Figure 4. Numerical SAR compared to the analytical SAR in the muscle sphere for 2 mm, 1 mm and 0.5 mm resolutions.

size of the sphere is comparable to the dimensions of small body parts such as hands or feet. The analytical electric field inside the sphere was calculated by a truncated Mie series, from which the whole-sphere averaged SAR was calculated by a spherical quadrature (available at: www.mathworks.com/matlabcentral/fileexchange/10750-quadrature-rules-for-spherical-volume-integrals). Basic staircase approximation was used to model the sphere in the FDTD. The Mie solution was calculated for a sphere with volume equal to that of the staircased sphere, so analytical solutions for different resolutions differ somewhat.

Local comparison of the analytical and numerical power loss is not possible on the surface of the sphere, where the analytical and numerical geometries are different. Because of this problem, the error in the localized power loss is approximated as

$$l_1 \text{ error} \approx \frac{\int |s_{\text{FDTD}} - s_{\text{analytical}}| \, \mathrm{d}V}{\int s_{\text{analytical}} \, \mathrm{d}V}, \tag{8}$$

where the integral is calculated numerically by a spherical quadrature (about 16 000 quadrature points) over the largest sphere which fits inside the staircased sphere. The FDTD power loss s_{FDTD} (assumed to be positioned at the centre points of the cells) is interpolated linearly to the quadrature points. Figure 4 shows the comparison between the analytical and numerical SAR in the frequency range from 500 MHz to 8 GHz for 2 mm, 1 mm and 0.5 mm resolutions. It seems that in this case either the linear or the mid-ordinate algorithm gives the best match with the analytical whole-sphere averaged SAR. Also, the mid-ordinate and linear algorithms have significantly smaller l_1 errors compared to the trapezium algorithm.

Unlike the 1D case, the mid-ordinate algorithm does not necessarily underestimate the analytical whole-sphere SAR, as is the case at the lower end of the frequency range and for high resolutions. However, similar to the 1D case, the trapezium algorithm always overestimates the whole-body SAR. Also, both the error in whole-sphere SAR and l_1 error do not seem to approach zero at low frequencies. This might be caused by the fact that the cubical grid is insufficient for representing the geometry correctly. So there is no doubt but that the electric field, and SAR, is incorrect near the surface of the sphere.

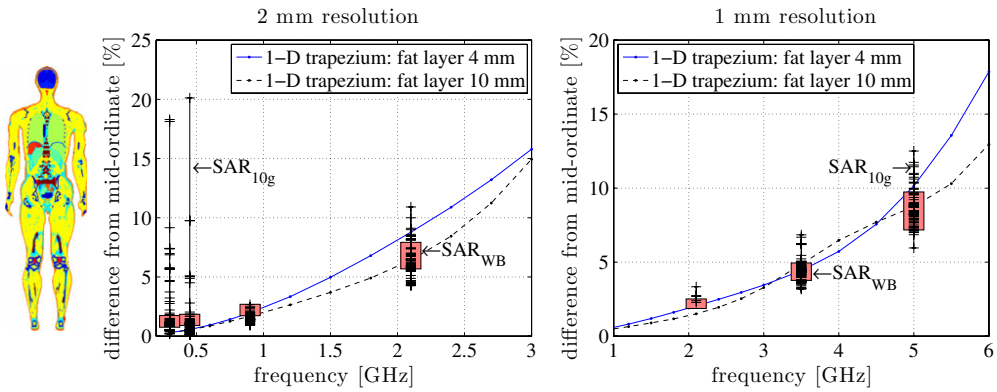

Figure 5. Trapezium algorithm compared to the mid-ordinate algorithm in heterogeneous body models. Total number of exposure cases is 240 for 2 mm resolution and 132 for 1 mm resolution. The bars show the difference in the whole-body averaged SAR between the algorithms varied over body models, incident directions and polarizations. Similar variation for 10 g SAR is shown by black vertical line segments, with each individual case marked by a short horizontal line segment. For comparison, the curves (SAR_{WB}) for the 1D case are calculated for the same kind of object as in figures 2 and 3, with skin thickness 2 mm and fat thicknesses 4 mm and 10 mm.

4. SAR calculations in realistic body models

In our previous paper (Uusitupa *et al* 2010), we studied the SAR in multiple human body models, ranging from an 18 kg boy to a 105 kg large man. Plane-wave exposure of both heterogeneous and homogeneous models was considered. In that study the SAR results were presented for the linear algorithm. In this study, the SAR results of 2 mm and 1 mm resolutions are examined also for the trapezium and mid-ordinate algorithms. Including all the incoming angles and horizontal and vertical polarizations, the total number of exposure cases is 684 (out of total 720). Heterogeneous models used in this paper include male adult, female adult and male child models from the Virtual Family (Christ *et al* 2010); Japanese adult male and female models (Nagaoka *et al* 2004); adult male NORMAN model (Dimbylow 1997) and the adult male model (only 1 mm resolution) based on the Visible Human Project (Mason *et al* 2000). Homogeneous models include homogenized versions of the male adult and child Virtual Family models, and an adult male model from the Poser software in standing, sitting, arms up and 'examine' postures. The number of incoming angles of the plane wave varies between the models (Uusitupa *et al* 2010).

Figures 5 and 6 show comparison between the SAR calculated by the trapezium and mid-ordinate algorithms for heterogeneous models and homogeneous models, respectively. The linear algorithm is approximately a weighted average (ratio 1:2) of the trapezium and mid-ordinate algorithms, so it is not shown for clarity. For comparison, the figures also show the ratios predicted by suitable 1D models (details in the figure captions).

The difference in whole-body averaged SAR values calculated by the different algorithms seems to be relatively independent of the variation of the used body model, incident angle and polarization, depending mainly on the frequency and resolution. This can be seen in figures 5 and 6, where the bars depicting the variation are short compared to the differences due to the frequency. Importantly, it seems that the 1D model is able to predict the whole-body SAR differences between the algorithms reasonably well in the whole frequency range, which is likely caused by somewhat similar dielectric properties in 1D and 3D models. The

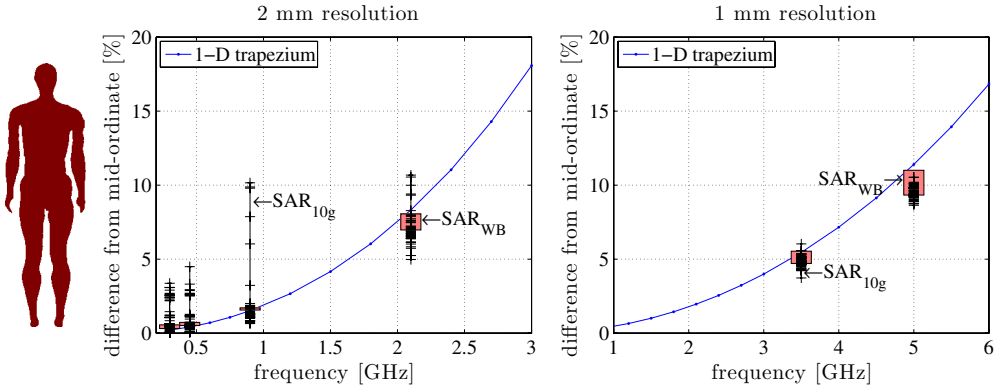

Figure 6. Trapezium algorithm compared to the mid-ordinate algorithm in homogeneous body models. Total number of exposure cases is 208 for 2 mm resolution and 104 for 1 mm resolution. The markings are similar to figure 5. One-dimensional object is homogeneous with dielectric properties a weighted average of muscle $(2/3)$ and fat $(1/3)$.

results agree fairly well with earlier results by Dimbylow *et al* (2008) (figure 12), but the difference between the SAR algorithms was slightly larger in that study. Dimbylow *et al* (2010) reported somewhat larger variability due to the SAR algorithm, which is likely to be caused by considerably higher permittivity and conductivity of newborn tissues. In this study, all the studied models had the same standard dielectric properties (Gabriel *et al* 1996).

In figures 5 and 6, the difference of maximum 10 g SAR seems to have a similar pattern with frequency as whole-body SAR, but the dependence on the model and exposure scenario is larger. The average difference of maximum 10 g SAR is typically close to the difference of whole-body SAR. However, in some special cases (marked by short horizontal line segments in figures 5 and 6) at the lower end of the frequency range the maximum relative difference may be as large as 20%. The large difference is because the maximum 10 g SAR is located in a body part where the SAR values are particularly sensitive to the calculation algorithm. There is seemingly a large difference at 900 MHz in the homogeneous case because in the five cases the maximum is located in the toes of the homogeneous Virtual Family adult male model. At 300 and 450 MHz, the 10 g SAR results are sensitive to the calculation algorithm in several cases in all of which the polarization is horizontal and the location of the maximum 10 g SAR value is in the armpits or in the groin.

Because the trapezium and mid-ordinate algorithms are based on elementary integration rules, the difference between the algorithms becomes larger with a steeper spatial rate-of-change in the electric field. Thus there is a large difference between the algorithms on the skin–air interface, where there are steep electric field gradients that are caused by the strong dielectric contrast together with the staircase approximation of the skin–air interface. High sensitivity of the SAR values in the toes, armpits or groin may be explained by the relatively large skin–air surface area in these body parts.

5. Conclusions

This paper presented three different algorithms for calculating the SAR in FDTD: the trapezium, mid-ordinate and linear algorithms. The properties of the algorithms were first investigated by comparing the numerical SAR values to analytic solutions in infinite 1D

layered objects and in a 3D muscle sphere. Finally, the algorithms were applied for dosimetry of anatomically realistic whole-body models.

The trapezium algorithm always gives a higher pointwise SAR than the mid-ordinate and linear algorithms. In all studied cases, the trapezium algorithm also overestimated the whole-body SAR compared to the analytic solution. Using too coarse resolution only amplified the overestimation of SAR. Hence, the trapezium algorithm is the most conservative choice for worst-case exposure assessment. One drawback of the trapezium algorithm is that it generally produced the worst match with the analytic solutions at high frequencies, where fine resolution is needed. An added benefit of the trapezium algorithm is that the discrete principle of conservation of energy, i.e. the discrete Poynting's theorem (de Moerloose and de Zutter 1995), is satisfied.

The mid-ordinate algorithm always gives a smaller pointwise SAR than both the trapezium and linear algorithms. Comparison with analytic solutions showed that the mid-ordinate algorithm had the tendency to almost always underestimate the accurate whole-body averaged SAR, and the underestimation was more severe for coarser resolutions. Hence, the mid-ordinate algorithm is not well suited for worst-case exposure assessment. The advantage of the mid-ordinate algorithm is that it usually gave a better fit with analytic SAR distribution at high frequencies compared to the trapezium algorithm.

The linear algorithm may produce either under- or overestimation of the whole-body SAR, depending on the case. It provides a reasonable trade-off between under- and overestimation as it is approximately a weighted average (1:2) of the trapezium and mid-ordinate algorithms. Although in some cases both the trapezium and mid-ordinate algorithms gave even better match with the analytic whole-body SAR, the linear algorithm was on average the most accurate (but not the most conservative) choice. Also, the linear algorithm generally provided the smallest error in the shape of the SAR distribution, allowing the use of lower resolution at slightly higher frequencies compared to the other two algorithms. The trapezium algorithm should be preferred in worst-case exposure assessment because it produces a conservative SAR estimate. But then, if better overall accuracy is required, the linear algorithm is preferred.

For studying the effects of the SAR calculation algorithms in realistic dosimetric calculations, a large number of different plane-wave exposure scenarios with various anatomically realistic body models were simulated. The whole-body SAR differences between different algorithms were relatively independent of the model, incident direction and polarization, depending mainly on the resolution and the frequency. The difference between the algorithms could be predicted by a suitable 1D layered model. So whole-body averaged SAR results calculated with various algorithms can be made inter-comparable by scaling the results accordingly. For example, the trapezium algorithm gives about 6–8% higher whole-body averaged SAR than the mid-ordinate algorithm in heterogeneous 2 mm models at 2100 MHz (figure 5), regardless of the model or exposure scenario. Increasing difference between the algorithms at higher frequencies is a sign of increasing discretization error in the FDTD method. In an ideal case, the SAR calculations could be performed using very fine resolution compared to the wavelength, and the difference between the algorithms would be negligible. However, due to computational limitations, practical SAR calculations are usually affected by some discretization error at high frequencies. Thus, the choice of the SAR calculation algorithm is an important simulation parameter, which should be explained to allow intercomparison of the results between different studies.

Acknowledgments

We thank GETA (Graduate School in Electronics, Telecommunication and Automation) for financial support. We thank CSC (Finnish IT Center for Science) for providing computational resources.

References

Caputa K, Okoniewski M and Stuchly M A 1999 An algorithm for computations of the power deposition in human tissue *IEEE Antennas Propag. Mag.* **41** 102–7

Christ A *et al* 2010 The virtual family—development of surface-based anatomical models of two adults and two children for dosimetric simulations *Phys. Med. Biol.* **55** N23–38

de Moerloose J and de Zutter D 1995 Poynting's theorem for the finite-difference-time-domain method *Microw. Opt. Technol. Lett.* **8** 257–60

Dimbylow P J 1997 FDTD calculations of the whole-body averaged SAR in an anatomically realistic voxel model of the human body from 1 MHz to 1 GHz *Phys. Med. Biol.* **42** 479–90

Dimbylow P, Bolch W and Lee C 2010 SAR calculations from 20 MHz to 6 GHz in the University of Florida newborn voxel phantom and their implications for dosimetry *Phys. Med. Biol.* **55** 1519–30

Dimbylow P J, Hirata A and Nagaoka T 2008 Intercomparison of whole-body averaged SAR in European and Japanese voxel phantoms *Phys. Med. Biol.* **53** 5883–97

Findlay R P and Dimbylow P J 2006 Variations in calculated SAR with distance to the perfectly matched layer boundary for a human voxel model *Phys. Med. Biol.* **51** N411–5

Gabriel S, Lau R W and Gabriel C 1996 The dielectric properties of biological tissues: III. Parametric models for the dielectric spectrum of tissues *Phys. Med. Biol.* **41** 2271–93

Kühn S, Jennings W, Christ A and Kuster N 2009 Assessment of induced radio-frequency electromagnetic fields in various anatomical human body models *Phys. Med. Biol.* **54** 875–90

Laakso I 2009 Assessment of the computational uncertainty of temperature rise and SAR in the eyes and brain under far-field exposure from 1 to 10 GHz *Phys. Med. Biol.* **54** 3393–403

Laakso I, Ilvonen S and Uusitupa T 2007 Performance of convolutional PML absorbing boundary conditions in finite-difference time-domain SAR calculations *Phys. Med. Biol.* **52** 7183–92

Mason P A, Hurt W D, Walters T J, D'Andrea J A, Gajsek P, Ryan K L, Nelson D A, Smith K I and Ziriax J M 2000 Effects of frequency, permittivity, and voxel size on predicted specific absorption rate values in biological tissue during electromagnetic-field exposure *IEEE Trans. Microw. Theory Tech.* **48** 2050–8

Nagaoka T, Watanabe S, Sakurai K, Kunieda E, Watanabe S, Taki M and Yamanaka Y 2004 Development of realistic high-resolution whole-body voxel models of Japanese adult males and females of average height and weight, and application of models to radio-frequency electromagnetic-field dosimetry *Phys. Med. Biol.* **49** 1–15

Roden J A and Gedney S D 2000 Convolution PML (CPML): an efficient FDTD implementation of the CFS-PML for arbitrary media *Microw. Opt. Technol. Lett.* **27** 334–9

Rylander T, Edelvik F, Bondeson A and Riley D 2005 Advances in hybrid FDTD-FE techniques *Computational Electrodynamics: The Finite-Difference Time-Domain Method* ed A Taflove and S C Hagness (Boston, MA: Artech House Publishers) pp 907–53

Taflove A and Hagness S C 2005 *Computational Electrodynamics: The Finite-Difference Time-Domain Method* 3rd edn (Boston, MA: Artech House Publishers)

Uusitupa T M, Ilvonen S A, Laakso I M and Nikoskinen K I 2008 The effect of finite-difference time-domain resolution and power-loss computation method on SAR values in plane-wave exposure of Zubal phantom *Phys. Med. Biol.* **53** 445–52

Uusitupa T, Laakso I, Ilvonen S and Nikoskinen K 2010 SAR variation study from 300 to 5000 MHz for 15 voxel models including different postures *Phys. Med. Biol.* **55** 1157–76

Wang J, Fujiwara O, Kodera S and Watanabe S 2006 FDTD calculation of whole-body average SAR in adult and child models for frequencies from 30 MHz to 3 GHz *Phys. Med. Biol.* **51** 4119–27